CHEMISTRY
A EUROPEAN JOURNAL

FULL PAPER

DOI: 10.1002/chem.201201384

Theoretical Assessment of Binding and Mass-Transport Effects in Electrochemical Affinity Biosensors That Utilize Nanoparticle Labels for Signal Amplification

Jie Zhang,*[a, b] Boon Ping Ting,[a] and Jackie Y. Ying*[a]

Abstract: This paper presents a theoretical study of electrochemical affinity biosensors for the detection of DNA/protein that utilize nanoparticle labels for signal amplification. This study analyzes the effects of binding and mass transport of the analytes on biosensor performance by using numerical simulations. Four cases were considered: 1) nanoparticles used to increase the loading of an electroactive species, or used as catalysts under pseudo-first-order conditions; 2) nanoparticles used as ultramicroelectrode arrays for the electrolysis of large concentrations of substrate; 3) nanoparticles used as seeds to deposit electrochemically detectable species; and 4) nanoparticles used to mediate the deposition of electrocatalysts. By using nanoparticle labels, high sensitivity is possible under all conditions considered. However, theoretical findings suggested that nonspecific adsorption could be more problematic in cases 2–4 due to the mismatch between the chemistry of surface binding and the principle of signal amplification that originates from the effect of mass transport. Under these conditions, any given signal would plateau at a much lower analyte concentration, well before the analyte binding had actually reached a plateau. Views on possible solutions to the above limitations are also presented.

Keywords: biosensors · electrochemical affinity · nanoparticles · surface chemistry · theoretical studies

Introduction

There is an increasing need for the development of simple, rapid, and ultrasensitive affinity biosensors for the detection of proteins and DNA.[1–4] These types of sensors are crucial for the rapid and early-stage diagnosis of diseases, for the detection of biological threats, and for drug screening. For such applications, the signal transducer surface of the biosensor is typically modified with biorecognition units such as the probe DNA or antibody. The probe can then selectively bind to the target analyte, such as a DNA molecule or cancer marker. However, it is difficult to directly detect such a binding event on account of the limited number of binding sites on the biosensor surface. To achieve high sensitivity, a signal amplification step is usually required. In the field of ultrasensitive electrochemical biosensors, this amplification step is very often achieved by using enzyme or nanoparticle labels.[5–7] In the latter case, nanoparticles have been used to increase the loading of electrochemically detectable species, or as catalysts for the electrolysis of large concentrations of substrate to enhance the sensitivity of the biosensor. Metallic nanoparticles and semiconductor quantum dots have been used for this purpose.[5–10] General procedures involved in the fabrication of this type of biosensor and its application in the detection of target biomolecules are shown schematically in Figure 1. The following steps are involved: 1) the conjugation of a capture probe at an optimal density to the electrode surface, 2) the capture of a target analyte, 3) the labeling of the bound analyte with a nanoparticle conjugated to an analyte-specific biomolecule, 4) the optional use of a further enhancement step by using a developer solution for the deposition of metal based on a seed-mediated nucleation/growth mechanism, and 5) detection in a separate solution.

Electrochemical detection of nanoparticles can be based on either their redox or catalytic properties. In general, strategies that utilize nanoparticle labels in electrochemical biosensors can be subcategorized into four main types (cases 1–4) with increasing complexity: 1) Nanoparticles can be used to increase electroactive species loading since every nanoparticle consists of thousands of atoms. Electrochemical techniques, such as stripping voltammetry and ion-selective electrodes, are used to detect the amplified signal from the dissolved ions.[11–20] Recently, solid-state voltammetry has also been used to directly detect Ag nanoparticle labels.[21,22] 2) The quantity of nanoparticles deposited may be indirectly measured on the basis of the catalytic current due to the electrolysis of a large quantity of substrate.[23–26] In this case, when nanoparticle labels are in close contact with the electrode surface (typically less than 2 nm) and in good electronic communication with the electrode surfaces, they can

[a] Dr. J. Zhang, B. P. Ting, Prof. Dr. J. Y. Ying
Institute of Bioengineering and Nanotechnology
31 Biopolis Way, The Nanos
Singapore 138669 (Republic of Singapore)
E-mail: jyying@ibn.a-star.edu.sg

[b] Dr. J. Zhang
School of Chemistry, Monash University
Clayton, Vic 3800 (Australia)
E-mail: jie.zhang@monash.edu

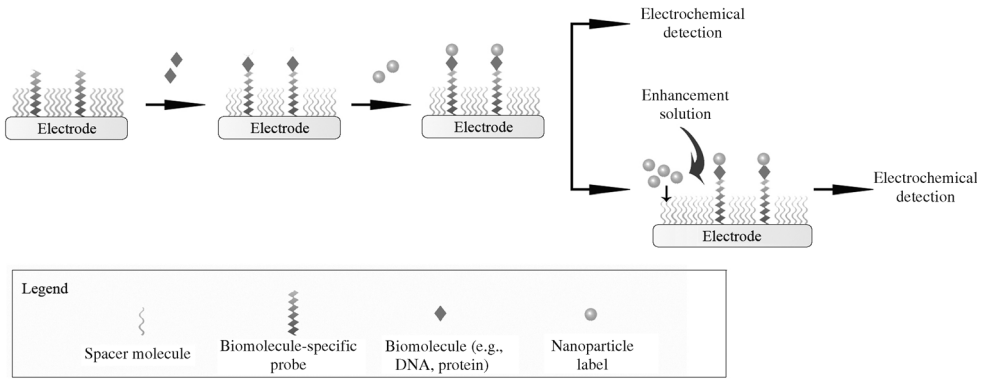

Figure 1. Schematic of the electrochemical affinity biosensor utilizing nanoparticles for signal amplification.

be used as ultramicroelectrode arrays for the electrolysis of large concentrations of substrate. Labels with high catalytic activity such as Au or Pt nanoparticles are ideal candidates. Since these noble metal catalysts are often highly stable toward electrooxidation, direct detection by stripping voltammetry might be difficult, thereby making the catalytic strategy a useful alternative. 3) Nanoparticles can be used as seeds to deposit electrochemically detectable species. This strategy is an extended configuration of the first strategy for signal amplification. This is very often achieved on the basis of a seed-mediated nucleation/growth mechanism by utilizing Ag or Au seeds to mediate the deposition of more Ag or Au. This strategy has been valuable in the design of ultrasensitive biosensors by many groups.[27–39] 4) Alternatively, nanoparticles can be used as catalysts to deposit more particles that possess catalytic activity, similar to the labels mentioned in strategy 2. The amount of particles deposited may be indirectly measured on the basis of their catalytic activity towards the electrolysis of a large quantity of substrates. This is particularly useful for developing a sandwich immunosensor. In this case, the nanoparticle labels are normally far away from the electrode surface and lack electronic communication with the electrode. Therefore, strategy 2 cannot be implemented for protein sensors. DNA or protein biosensors developed on the basis of strategy 4 have not been fully demonstrated. However, Huang et al. have formulated a human immunoglobulin G (hIgG) sensor based on the inhibition of Pt catalytic activity in the presence of copper deposition. When a detection antibody conjugated with alkaline phosphatase binds to hIgG, the enzyme catalyzes the hydrolysis of ascorbic acid, which in turn mediates the deposition of copper onto a Pt electrode surface. The resulting shift in the potential for the catalytic reduction of protons by the Pt electrode can then be measured. This allows for an indirect quantification of the amount of Cu deposited, which can then be related to the hIgG concentration.[40]

The amplified sensing strategies described above, which range from the simple electrochemical detection of nanoparticle labels to the complex electrochemical detection of deposited electroactive species or electrocatalyst, are indeed remarkable. Signal amplification has allowed for the detection of sub-femtomolar concentrations of biomolecules. The performance of this type of electrochemical biosensor (configured as in Figure 1) can be influenced at least by the binding and mass transport of the analytes. The combination of these effects leads to an extremely complex mathematical problem whereby the analytical solutions cannot be easily obtained. Consequently, the relationships between the electrochemical signal, analyte concentration, and biosensor sensitivity, and the implications of utilizing signal amplification strategies are still unclear to experimental electrochemists, and a quantitative theory on this subject would be very helpful. Unfortunately, despite the abundance of publications on protein and DNA biosensors, theoretical papers are rare. Notably, Savéant and co-workers have investigated the performance of electrochemical biosensors based on enzymatic amplification strategies under conditions whereby complex mass transport can be omitted.[41,42] Therefore, analytical solutions of the problem related to the theoretical biosensor performance could be obtained. To date, theoretical studies on the performance of electrochemical biosensors based on nanoparticle amplification strategies have not been reported to our knowledge.

In this paper, we have considered the influence of surface chemistry and mass transport on biosensor responses. The aim of this paper was 1) to provide a theoretical basis for the evaluation of sensor performance, including sensitivity, detection limit, and dynamic range, 2) to predict the key features, specifically the possible drawbacks, associated with each sensing strategy, and 3) to provide guidance for biosensor design. To achieve these goals, numerical simulations were used to address these theoretical problems, and to obtain the theoretical biosensor response. This paper also discusses the analytical performance of biosensors, and the implications of signal amplification. Possible solutions to these limitations are also suggested.

Theoretical Methods

To obtain theoretical responses for electrochemical affinity biosensors, three key factors must be considered.

Adsorption isotherm: In an affinity biosensor, only those target analytes that bind to the biosensor surface would contribute to the biosensor re-

sponse. Therefore, one would expect that the adsorption isotherm[43] of the analytes would have a profound effect on the biosensor performance, especially on the relationship of the biosensor response versus the logarithmic value of the analyte concentration (i.e., the calibration curve for affinity biosensors). We consider both the Langmuir isotherm [Eq. (1)] and Frumkin isotherm [Eq. (2)] for surface-binding processes. The Langmuir isotherm is the simplest adsorption isotherm. It assumes the surface to be homogeneous, and every binding process to be independent and identical. In contrast, whereas the Frumkin isotherm also assumes the surface to be homogeneous, it further considers the interaction between the adsorbed species. When repulsion between the adsorbed species is present, α is negative. When attraction between the adsorbed species exists, α is positive. If α is zero, Equation (2) has the same form as Equation (1), which implies that there is no interaction between the adsorbed species.

$$\text{Langmuir isotherm}: \ \theta = \frac{Kc}{1+Kc} \tag{1}$$

$$\text{Frumkin isotherm}: \ \theta = \frac{Kc\exp(\alpha\theta)}{1+Kc\exp(\alpha\theta)} \tag{2}$$

in which θ = the surface coverage of the adsorbed species, K = the affinity constant, and c = the concentration of the adsorbed species in the solution phase.

In the analysis of a real sample, capture probes, target analytes, and labels would adsorb onto the surface. Therefore, the calibration curve is expected to be affected by the adsorption behavior of these species. Since the capture probe is usually conjugated to the electrode surface by covalent binding, K is ideally infinitely large. In the labeling step in which the surface-bound target analyte is labeled with a nanoparticle-conjugated analyte-specific biomolecule, a large concentration of the label is used to ensure that each target analyte is tagged with a label. Therefore, the adsorption behavior of the label has a minimal effect on the biosensor calibration curve. Consequently, the calibration curve is governed primarily by the adsorption behavior of the target analyte to the capture antibody.

For the convenience of data analysis, the following numerical simulations will assume that each analyte molecule is consistently labeled with one nanoparticle label regardless of its surface coverage, assuming that there is sufficient room on the electrode surface for the labels, unless otherwise stated. In all calculations, we also assume that there is a maximum of 4×10^{10} target analyte molecules on a 2 mm-diameter electrode. Consequently, if the labeling nanoparticle is 10 nm in diameter, the nanoparticle labels would cover the electrode surface completely when the surface coverage of the analyte is 1. Furthermore, 1) if the nanoparticle is smaller than 10 nm in diameter, the nanoparticle labels would only cover part of the electrode surface when the surface coverage of the analyte is 1, and 2) if the nanoparticle is larger than 10 nm in diameter, the nanoparticle labels would reach full surface coverage before the target analyte achieves full surface coverage. For example, nanoparticle labels with a diameter of 20 nm would have a full surface coverage when the analyte molecules cover only 25% of the surface.

Effect of mass transport: Two types of electrode processes are encountered in this study. The first type is the electrolysis of the substrate. This type of process is associated with the detection step in cases 2 and 4 (see the Introduction). A reversible process described by Equation (3) is considered here.

$$\mathrm{Ox} + ne^- \underset{k_b}{\overset{k_f}{\rightleftharpoons}} \mathrm{Red} \tag{3}$$

In this reaction, Ox and Red are the oxidized and reduced forms, respectively, whereas k_f and k_b are the heterogeneous forward and reverse rate constants for the electron-transfer step. The electron-transfer process that is assumed is as described by the Butler–Volmer relationship [Eq. (4)]:[43]

$$k_f = k^{0'}\exp\left[\frac{-\beta nF}{RT}\left(E-E^{0'}\right)\right] \text{ and } k_b = k^{0'}\exp\left[\frac{(1-\beta)nF}{RT}\left(E-E^{0'}\right)\right] \tag{4}$$

in which E is the potential of the working electrode versus the reference electrode (controlled by using a potentiostat), $E^{0'}$ is the reversible potential, $k^{0'}$ is the formal electron-transfer rate constant at potential $E^{0'}$, β is the electron-transfer coefficient, F is the Faraday constant, R is the gas constant, and T is the temperature.

In the second type of electrode process studied, nanoparticles are used as seeds to mediate the deposition of an electroactive species (case 3) or nanoparticle electrocatalysts (case 4). The electrode reaction that models this metal-deposition process is described in Equation (5),

$$\mathrm{M}^{n+} + ne^- \rightarrow \mathrm{M} \tag{5}$$

In this case, the potential on the surface of the nanoparticle is controlled by the solution-phase electroactive species on the basis of the mixed potential theory.[44]

Mass transport is important in electrochemical studies since the electrode reaction is a heterogeneous reaction.[43] In cases 2–4, every nanoparticle seed can be considered an ultramicroelectrode. As shown in Figure 2, when the analyte concentration increases, analyte surface coverage also increases. Thus, the increased density of the nanoparticle labels leads to an increase in diffusion layer overlap, which in turn affects the sensor response. In the quantitative simulation of the theoretical responses in cases 2–4, three simplifications are made. 1) All nanoparticles are represented using nanodiscs with the same diameter as the nanoparticles, and are considered to be uniformly distributed on the electrode surface. 2) In the case of dominant radial diffusion, the double-layer effect[45,46] is ignored. As will be shown later, the biosensor response at the analyte concentration range whereby radial diffusion is dominant is not of interest since it falls outside the dynamic range of the biosensor. 3) For the same consideration, the electrode reaction is assumed to be reversible. The electrochemical process will not be considered reversible when radial diffusion is dominant because of the extremely high mass-transport rate associated with nanoparticulate electrodes.

In the presence of a sufficient amount of supporting electrolyte, the mass transport of an electroactive species is governed by Fick's law of diffusion [Eq. (6)]:[43,47]

$$\frac{\partial c_i}{\partial t} = D_i\left(\frac{\partial^2 c_i}{\partial r^2} + \frac{1}{r}\frac{\partial c_i}{\partial r} + \frac{\partial^2 c_i}{\partial z^2}\right) \tag{6}$$

in which t = time, D_i and c_i (i = Red or Ox) are the diffusion coefficient and concentration of the reduced or oxidized species, respectively, and r and z are the radial and normal coordinates to the electrode surface, respectively. The definition of the coordinate system used for the ultramicrodisc electrode of interest is shown in Figure 2.

Equation (6) can be solved by using the following initial and boundary conditions.

At $t=0$, for all z and all r [Eq. (7)]:

$$c_{\mathrm{Ox}} = c^*_{\mathrm{Ox}},\ c_{\mathrm{Red}} = 0 \tag{7}$$

At $t>0$, for $r=0$ or $r=R$ and all z [Eq. (8)]:

$$D_i\frac{\partial c_i}{\partial r} = 0 \tag{8}$$

For $z=\infty$ and all r [Eq. (9)]:

$$c_{\mathrm{Ox}} = c^*_{\mathrm{Ox}},\ c_{\mathrm{Red}} = 0 \tag{9}$$

For $z=0$, $a<r\le R$ [Eq. (10)]:

$$D_i\frac{\partial c_i}{\partial z} = 0 \tag{10}$$

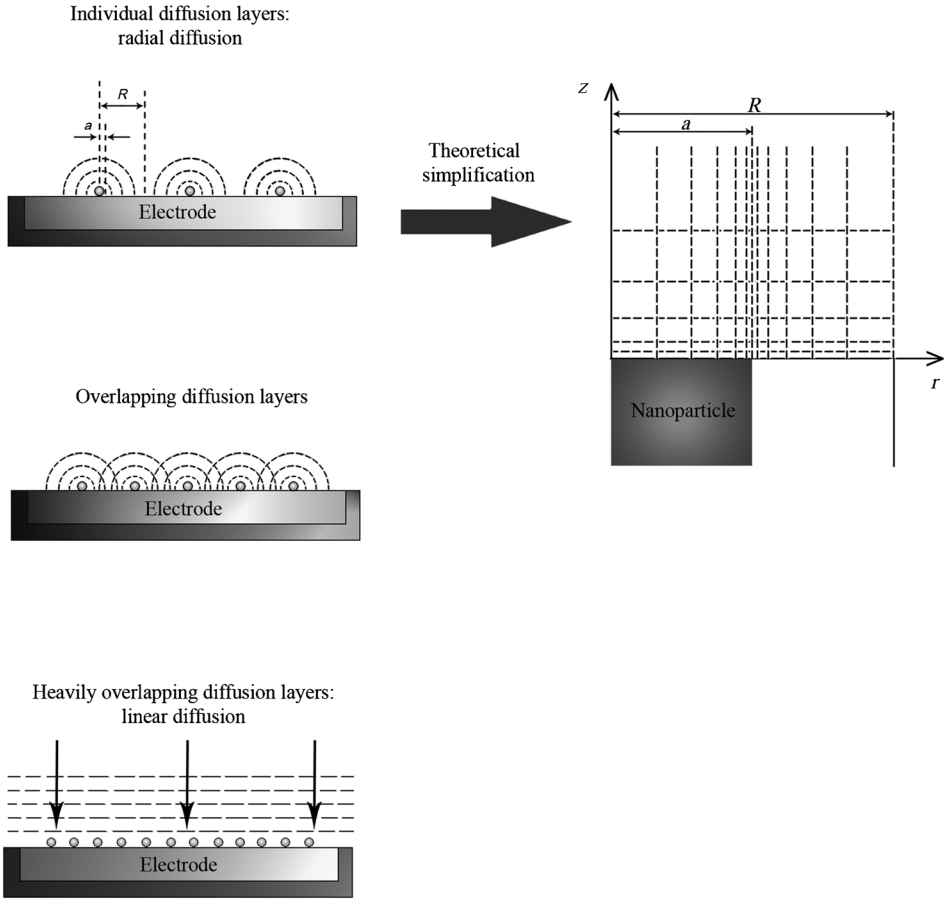

Figure 2. Schematic of the effect of mass transport on the biosensor response and the coordinate system for the nanoparticle represented using an ultramicrodisc in the theoretical calculations, in which a = radius of the nanoparticle and R = radius of the area occupied by each nanoparticle.

For $z = 0$, $0 < r \leq a$ [Eq. (11)] in the case of substrate electrolysis:

$$-D_{Ox}\frac{\partial c_{Ox}}{\partial r} = D_{Red}\frac{\partial c_{Red}}{\partial r} = k_f c_{Ox} - k_b c_{Red} \quad (11)$$

and in the case of seed-mediated nucleation/growth [Eq. (12)]:

$$c_{Ox} = 0 \quad (12)$$

Due to the application of a large concentration of strong reducing agent in the developer solution, the concentration of the metal ions on the nanoparticle surface is expected to be negligible on the basis of the mixed potential theory.[44]

In the above equations, cc^{*}_{Ox} = the bulk concentration of the oxidized species. Equation (3) is solved to obtain time- and spatial-dependent concentrations using the alternating direction implicit finite difference method.[48] The current density along the edge of the ultramicrodisc electrode is significantly higher in the case in which radial diffusion contributes significantly to the mass transport.[49] To accurately calculate the Faradaic current under conditions of a nonuniform current density, an expanding space grid,[50] as shown in Figure 2, is used. This helps to achieve highly accurate numerical simulations without losing efficiency. This approach has been previously adopted in the simulation of the Faradaic response at ultramicrodisc,[48,51] microring,[52] and tubular band[53] electrodes.

The current, I, can be calculated according to Equation (13) once the space- and time-dependent concentration is known at any potential:

$$I = 2\pi nFD_{Ox}\int_0^a \left(\frac{\partial c_{ox}}{\partial z}\right)_{z=0} r\,dr \quad (13)$$

A numerical simulation of this type has been conducted by Compton and co-workers in the context of a partially blocked electrode.[54–59] Herein it is applied to the systems of interest for this study.

In the case of the seed-mediated nucleation/growth process, the total charge, Q, involved in the electrode reaction can be obtained by integrating the time-dependent current [Eq. (14)]:

$$Q = \left|\int_0^t I\,dt\right| \quad (14)$$

Next, the amount (moles) of metal atoms, N, deposited can be calculated based on Faraday's law [Eq. (15)]. The number of nanoparticles deposited onto the electrode surface can then be obtained if the number of atoms per nanoparticle is known.

$$N = \frac{Q}{nF} \quad (15)$$

Seed-mediated nucleation/growth: The kinetics and mechanisms of electrode and electrodeless deposition of metal have been extensively investigated.[44,60] However, there is no quantitative theory on the effect of neighboring nanoparticles during the deposition process in the timescale whereby the diffusion layer of the individual nanoparticles begins to overlap. This type of problem is very complicated in terms of chemistry and mathematics. Electrodeless deposition is more often termed seed-mediated nucleation/growth in biosensor applications. The seed-mediated nucleation/growth process is possibly one of the most complicated processes.[61–65] Jana et al. reported that under different conditions, the seed-mediated process could either result in the growth of larger nanoparticles on the original seeds, or in the generation of additional seeds. They found that under the fast addition of reducing agent, the presence of seeds appeared to promote the formation of more seeds instead of particle growth. The observed nucleation was the dominant process compared to particle growth. They also found that the presence of a low concentration of seeds also favored the nucleation process. When seed-mediated processes are applied to the biosensing protocol for the purpose of signal amplification, a relatively high concentration of strong reducing agent is used together with a metal ion concentration of several millimolar with a relatively small number of seeds present on the electrode surface. Under these conditions, the main role of the seeds is to mediate the nucleation of an increasing number of seeds. Therefore, in our theoretical simulation, we have made the following simplifications. 1) The seed-mediated reduction of metal ions by the reductant is diffusion-controlled. 2) The seed-mediated metal ion reduction only occurs due to the original seeds, despite the possibility for new seeds to mediate the nucleation/growth of more seeds. 3) The seeds produced are monodispersed in size. 4) All of the seeds generated are deposited onto the electrode surface.

Results

In this section, numerical simulations were used to obtain the theoretical biosensor response under the four cases discussed above.

Case 1—Nanoparticles used to increase the loading of electroactive species: In this case, mass transport had no effect on biosensor response. Therefore, the analytical signal was expected to be proportional to the number of labels. The calibration curve was predicted to have exactly the same trend as the adsorption isotherm. The adsorption isotherm/normalized calibration curves (the biosensor responses were normalized with its maximum response) based on the Langmuir isotherm [Eq. (1)] are shown in Figure 3a. The binding

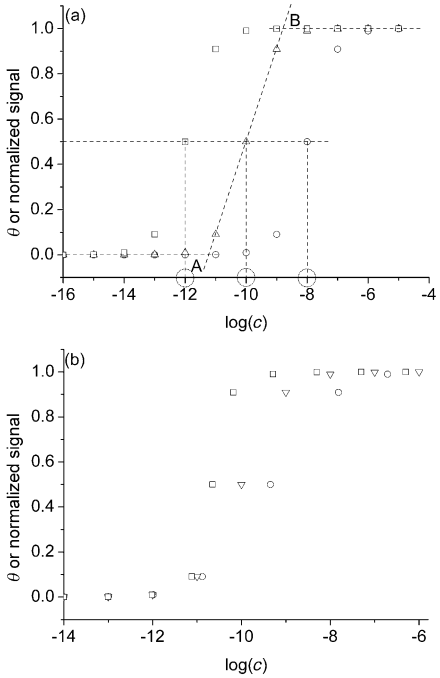

Figure 3. Dependence of θ or normalized signal on log(c) calculated on the basis of a) Langmuir isotherm for $K=(\bigcirc)\ 1\times10^{8}$, $(\Delta)\ 1\times10^{10}$, and $(\square)\ 1\times10^{12}\,\text{M}^{-1}$; and b) Frumkin isotherm for $K=1\times10^{10}\,\text{M}^{-1}$, and $\alpha=(\bigcirc)\ -3$, $(\bigtriangledown)\ 0$, and $(\square)\ 3$.

affinity constants of antigen to capture antibody were 1×10^{8}, 1×10^{10}, and $1\times10^{12}\,\text{M}^{-1}$. To obtain these curves, the theoretical calculation involved the following steps. 1) The concentration-dependent coverage of analytes based on the Langmuir isotherm was calculated. 2) The number of analytes on a 2 mm-diameter electrode, based on the known coverage, was calculated. 3) The number of nanoparticle labels was obtained based on a 1:1 equivalency to the amount of analyte. For analyte detection, the most suitable concentration range was the linear region of the calibration curve. This concentration range is typically called the dynamic range for affinity biosensors. The concentration range that showed linearity within the signal versus log(c) curve was governed by the nature of the binding event. The concentration that corresponds to the midpoint of the linear region of the calibration curve was the reciprocal of the adsorption affinity constant. The stronger the binding, the more sensitive the method would be. The signal versus log(c) curve has a linear range (see the concentration range between A and B in Figure 3a) over 3 to 4 orders of magnitude for the analyte concentration. The Langmuir isotherm assumes that every individual binding process is the same and unaffected by neighboring species. This assumption might not be suitable in the case of an affinity biosensor since the size and charge number of the analyte are relatively large. In this case, the Frumkin isotherm, which considers the interaction between the adsorbed species, might be a better approximation. Figure 3b shows the comparison of the results obtained based on the Frumkin and Langmuir isotherms. Although the linear range was wider, the sensitivity of the method (the slope of the curve) was lower when there was repulsion between the adsorbed species. An opposite effect was indicated in Figure 3b when there was attraction between the adsorbed species.

Another instance involved nanoparticles used as catalysts for the mediated electrolysis of a large concentration of substrates. By using an electron-transfer mediator under pseudo-first-order conditions whereby the change in the substrate concentration is negligible, biosensor responses due to the catalytic current under steady-state conditions were expected to be proportional to the number of nanoparticle label catalysts, and therefore to the amount of analytes on the electrode surface. In this case, the above conclusions were also applicable.

In an affinity biosensor, signals were plotted versus log(c) instead of c since one might expect that there is a significant analyte surface coverage in the dynamic range. As shown in Figure 3, this is true in case 1 whereby the effect of mass transport can be omitted. Therefore, the calibration curve is fully matched with the adsorption isotherm. However, it will be shown later in cases 2–4 that this might not be applicable once mass transport plays a role.

Case 2—Nanoparticles used as ultramicroelectrode arrays for the electrolysis of a large concentration of substrates: In this case, the theoretical calculation involved the following steps. 1) The concentration-dependent coverage of analytes based on the Langmuir isotherm was calculated. 2) The amount of analytes on a 2 mm-diameter electrode, based on the known coverage, was calculated. 3) The number of nanoparticle labels, which is equivalent to the amount of analytes, was obtained. 4) The area per particle was calculated. 5) The radius of the area occupied by one nanoparticle was calculated. 6) The response of an individual nanoparticle was simulated. Once the response of the individual nanoparticle was known, we could calculate the response of the biosensor and obtain the calibration curve. Figure 4 shows the typical voltammetric response of an individual 10 nm nanoparticle at different surface coverages when the diffusion coefficient and the substrate concentration were $1\times10^{-5}\,\text{cm}^{2}\,\text{s}^{-1}$ and 10 mM, respectively. When the coverage in-

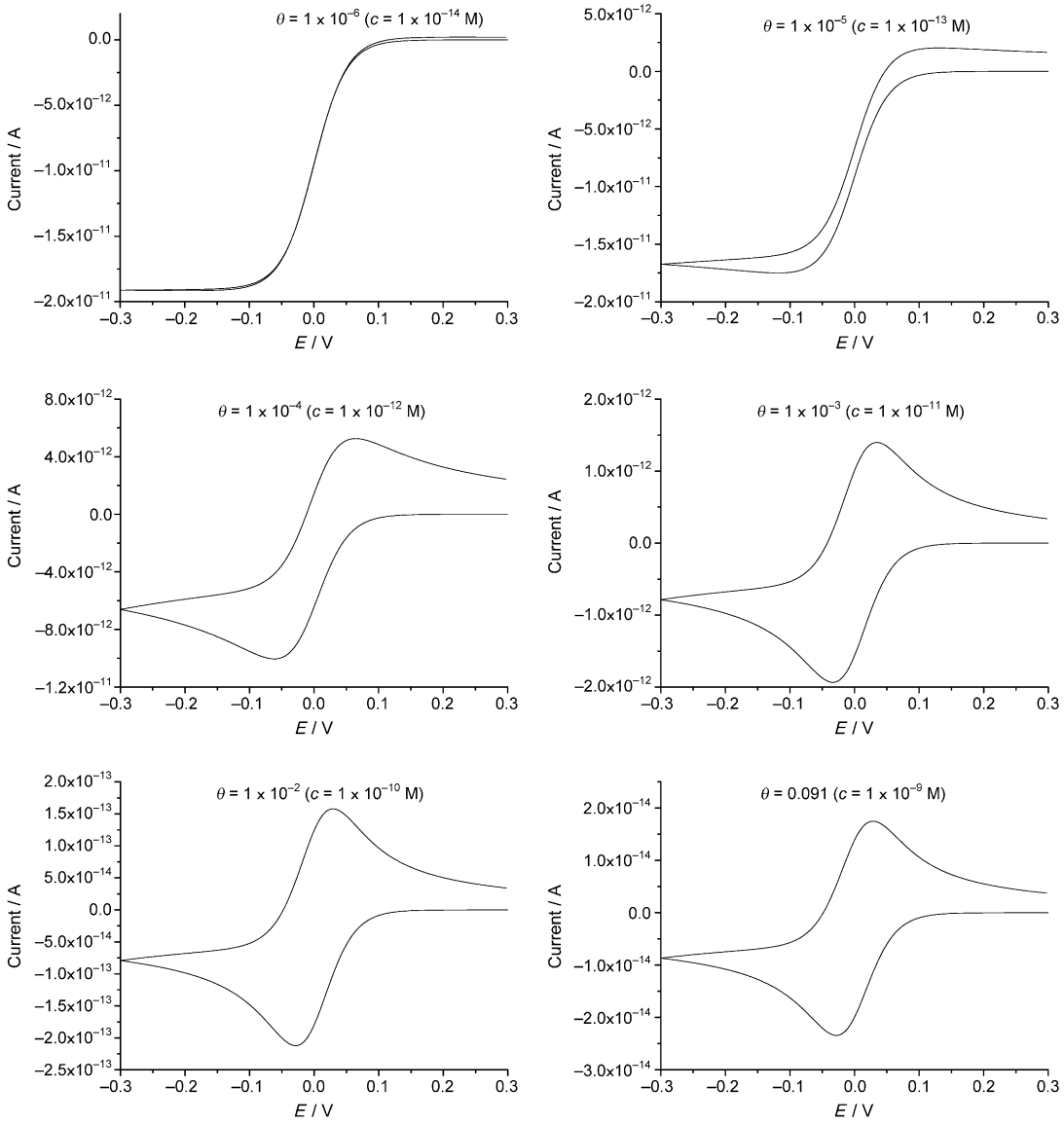

Figure 4. Response of a 10 nm-diameter nanoparticle when nanoparticles are used as ultramicroelectrode array for the electrolysis of a large substrate concentration (10 mM). $K = 1 \times 10^8\,\mathrm{M}^{-1}$, $D = 1 \times 10^{-5}\,\mathrm{cm^2\,s^{-1}}$, and scan rate $= 0.1\,\mathrm{V\,s^{-1}}$.

creased, the voltammetric characteristics changed from the steady-state sigmoidal shape to the transient peak shape. Additionally, the current magnitude from an individual nanoparticle decreased on account of the increasing level of overlap between the diffusion layers around the nanoparticle seeds. However, since the density of the nanoparticle labels increased at high concentrations, the overall peak current still increased to reach a plateau at high concentrations as shown in Figure 5.

In this case, the dynamic range of the calibration curve was very similar to that of the adsorption isotherm. However, the dynamic range was no longer determined solely by the adsorption isotherm, but also by mass transport. These results also showed that the use of nanoparticle labels could effectively enhance the sensitivity of the biosensor. This was achieved not only by increasing the magnitude of the signal through the electrolysis of a large substrate concentration, but also by moving the entire dynamic range towards a lower concentration.

The results in Figure 5 also showed that when the diffusion coefficient of the substrate increased, the absolute value of the signal also increased. Moreover, the dynamic range moved towards a lower concentration range on account of the increase in the mass-transport rate. These results were expected because of 1) the magnitude of the current would increase according to Equation (13), and 2) the diffusion field overlap would occur at a lower coverage of the nanoparticle labels, and thus, at a lower analyte concentration, when the diffusion coefficient of the substrate increased. Although we assume the substrate undergoes a reversible electrochemistry, the conclusions reached are also applicable to cases in which the substrate undergoes an irre-

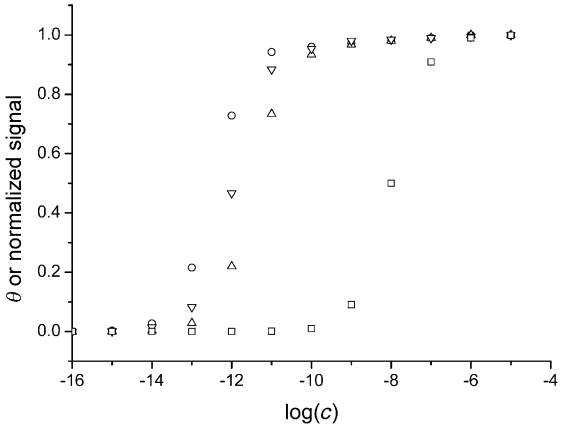

Figure 5. Effect of diffusion on the calibration curves of the biosensor when nanoparticles are used as ultramicroelectrode array for the electrolysis of a large substrate concentration (10 mM). $K=1\times10^{8}\,M^{-1}$; $D=$(○) 1×10^{-4}, (▽) 1×10^{-5}, and (Δ) $1\times10^{-6}\,cm^{2}s^{-1}$; scan rate $=0.1\,V s^{-1}$. A Langmuir isotherm (□) obtained with the same K value is also shown for comparison.

versible electrochemistry or a reaction catalyzed by the metal nanoparticles, as long as the process is controlled by diffusion.

Case 3—Nanoparticles used as seeds to deposit electrochemically detectable species: In case 3, the theoretical calculation involved the following steps. 1) The concentration-dependent coverage of analytes based on the Langmuir isotherm was calculated. 2) The amount of analytes on a 2 mm-diameter electrode based on the known coverage was calculated. 3) The number of nanoparticle labels, which was equivalent to the amount of analytes, was obtained. 4) The area per particle was calculated. 5) The radius of the area occupied by one nanoparticle was calculated. 6) The time-dependent current contributed by an individual nanoparticle under diffusion-controlled conditions was simulated. 7) The current-time curve was integrated to obtain the total charge involved during the deposition. 8) The total amount of electroactive species deposited was proportional to the total charge involved, as suggested by Faraday's law [Eq. (15)]. The biosensor response due to an individual nanoparticle seed was proportional to the amount of electroactive species deposited. Once the response of the individual nanoparticle seeds was known, we could calculate the response of the biosensor and obtain the calibration curve. Figure 6 depicts the typical current–time curve for an individual 10 nm nanoparticle at an analyte concentration of 1×10^{-13} M, $n=2$, and diffusion coefficient and concentration of the metal ions of $5\times10^{-6}\,cm^{2}s^{-1}$ and 0.5 mM, respectively. The area underneath the curve represented the total charge consumed [Eq. (14)], whereas the amount of deposition was calculated based on Equation (15). The calibration curve obtained with different deposition times is shown in Figure 7. The results again demonstrated that the dynamic range of the calibration curve was very similar to that shown in case 2. The dynamic range resulted from the effect of mass transport in

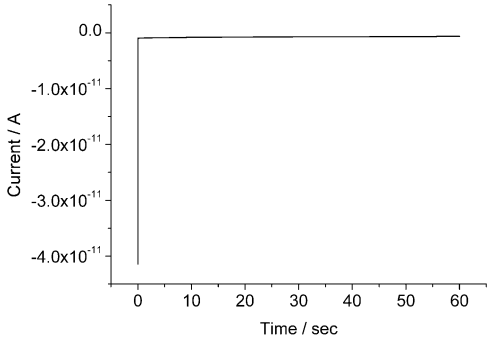

Figure 6. A typical current/time curve of an individual 10 nm-diameter nanoparticle. The nanoparticles are used as seeds to deposit electrochemically detectable species. The analyte concentration is 1×10^{-13} M, and the diffusion coefficient and concentration of metal ions are $5\times10^{-6}\,cm^{2}s^{-1}$ and 1 mM, respectively.

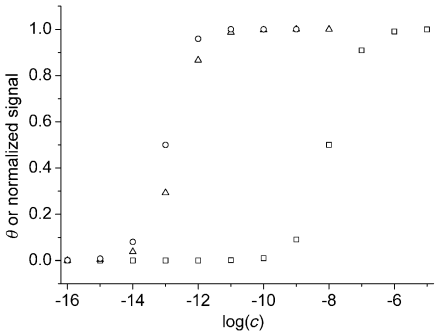

Figure 7. Effect of the deposition time on the calibration curves of the biosensor. Nanoparticles are used as seeds to deposit electrochemically detectable species. $K=1\times10^{8}\,M^{-1}$, and the diffusion coefficient and concentration of the metal ions are $5\times10^{-6}\,cm^{2}s^{-1}$ and 1 mM, respectively. Deposition time is ○) 5 min and Δ) 1 min. □) A Langmuir isotherm obtained with the same K value is also shown for comparison.

addition to the adsorption isotherm. In case 3, the results also showed that the use of nanoparticle labels could effectively enhance the sensitivity of the biosensor, not only by increasing the magnitude of the signal due to the presence of a large substrate concentration, but also by pushing the dynamic range towards a lower concentration range. These findings also suggested that although the increase in metal-deposition time was expected to increase the absolute value of the signal, the dynamic range was not significantly affected by the deposition time in this timescale. No significant shift in the dynamic range towards lower concentrations occurred with a deposition time of approximately 30 min (results are not shown). This was expected, since the diffusion layer thickness would be proportional to the square root of time,[43] hence a 30-fold increment from 1 to 30 min would only result in a less than 6-fold increment in the diffusion-layer thickness.

Case 4—Nanoparticles used to mediate the deposition of electrocatalysts: In case 4, nanoparticles were used to mediate the deposition of electrocatalysts. In this case, we followed steps 1–8 of the theoretical calculation procedure in

Table 1. Typical numbers of nanoparticles deposited onto the surface of a 2 mm-diameter electrode at different analyte concentrations. $K = 1 \times 10^{-8}$ M^{-1}, and the diffusion coefficient and concentration of metal ions are 5×10^{-6} cm^{2}s^{-1} and 0.5 mM, respectively.

Analyte concentration [M]	Analyte surface coverage	Number of nanoparticle labels[a]	Amount of charge involved with each nanoparticle label in 1 min [C]	No. of nanoparticles deposited onto the electrode surface[b]
1×10^{-18}	1×10^{-10}	4	5.8×10^{-11}	2.0643×10^{4}
1×10^{-17}	1×10^{-9}	40	5.8×10^{-11}	2.06425×10^{5}
1×10^{-16}	1×10^{-8}	400	5.8×10^{-11}	2.06425×10^{6}
1×10^{-15}	1×10^{-7}	4000	5.8×10^{-11}	2.06425×10^{7}
1×10^{-14}	1×10^{-6}	40000	5.66357×10^{-11}	2.01917×10^{8}
1×10^{-13}	1×10^{-5}	400000	4.38232×10^{-11}	1.56237×10^{9}
1×10^{-12}	1×10^{-4}	3.9996×10^{6}	1.2949×10^{-11}	4.61611×10^{9}
1×10^{-11}	9.99×10^{-4}	3.996×10^{7}	1.47624×10^{-12}	5.25782×10^{9}
1×10^{-10}	0.0099	3.9604×10^{8}	1.5039×10^{-13}	5.3086×10^{9}
1×10^{-9}	0.09091	3.63636×10^{9}	1.64392×10^{-14}	5.32811×10^{9}

[a] The diameter of the nanoparticle label is 10 nm. [b] Assumptions: the metal deposition is a reduction process that involves two electrons; the diameter of the nanoparticle deposited is 10 nm; and each nanoparticle contains 35000 atoms.

case 3 to obtain the amount of deposition. Once the amount of deposition was known, we could calculate the total number of nanoparticles deposited and the radius of the area occupied by one nanoparticle. Typical values for the number of nanoparticles deposited onto the surface of a 2 mm electrode at different analyte concentrations are listed in Table 1 for diffusion coefficient and metal ion concentration of 5×10^{-6} cm^{2}s^{-1} and 0.5 mM, respectively. The results suggested that by using seed-mediated deposition, a large quantity of nanoparticle electrocatalysts could be deposited onto the electrode in a short period of time. Once the number of nanoparticles was known, the area per particle and the radius of the area occupied by one nanoparticle could be calculated. The response of an individual newly seeded nanoparticle on the electrode surface could be simulated in the same way as in case 2, assuming that the presence of the nanoparticle labels had no effect on the biosensor response. Next, the overall biosensor response could be calculated once the response of the individual nanoparticle was known. Figure 8 shows the calibration curve of a biosensor ($K = 1 \times 10^{8}$ M^{-1}) that uses 10 nm nanoparticle labels to deposit nanoparticle electrocatalysts with a diameter of 10 nm, with voltammetric measurements conducted at a scan rate of 0.1 V s^{-1} in a solution that contained 10 mM of substrate ($D = 1 \times 10^{-5}$ cm^{2}s^{-1}). A Langmuir isotherm obtained with the same K value was also shown for comparison. The dynamic range of the calibration curve has been shown to be further shifted towards the lower concentration region than the examples shown in cases 2 and 3, on account of the effect of mass transport during both metal deposition and substrate electrolysis.

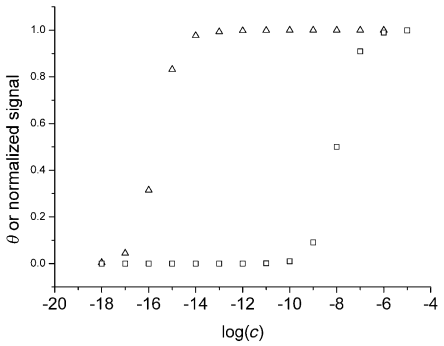

Figure 8. Δ) Calibration curve of the biosensor when nanoparticles are used to mediate the deposition of electrocatalysts. $K = 1 \times 10^{8}$ M^{-1}, diameter of the nanoparticle labels and newly seeded nanoparticles = 10 nm. Voltammetric measurements are conducted with a scan rate of 0.1 V s^{-1} in a solution containing 10 mM of substrate ($D = 1 \times 10^{-5}$ cm^{2}s^{-1}). □) A Langmuir isotherm obtained with the same K value is also shown for comparison.

Discussion

From the above results, one would conclude that in all cases, nanoparticle labels could greatly amplify the signal of electrochemical biosensors. Signal amplification occurred not only on account of the increase in signal magnitude, but also the shifting of calibration curve towards lower concentration, as in cases 2–4. However, there was a significant mismatch between the calibration curve of the biosensor and the adsorption isotherm. The calibration curve reached a plateau at a much lower analyte concentration, well before the adsorption isotherm reached a plateau. In the following, we discuss the possible implications of this effect, among others, on the biosensing of real samples by using electrochemical affinity biosensors.

Dynamic range and its origin: The above results suggested that the dynamic range was determined either by the adsorption isotherm, or the combined effect of the adsorption isotherm and the mass transport in the different biosensing strategies. When mass transport was not considered to be important, the dynamic range could be affected by the interaction of molecules on the surface. Depending on the type of interaction, the dynamic range could become larger or smaller. Conversely, in a biosensor whereby the adsorption isotherm and mass transport both played an active role, its dynamic range would be very similar to the case whereby the Langmuir isotherm was the sole determining factor. In the case whereby the dynamic range was controlled by the adsorption isotherm and mass transport, the interaction be-

tween the nanoparticle seeds when the analyte concentration was within the dynamic range was expected to be small due to their low surface coverage (≤ 0.1 in cases 2–4 considered above). Therefore, a simple Langmuir isotherm appeared to be a good model to describe the surface adsorption processes in this range. Unfortunately, nonspecific adsorption of labels on the free surface would also become problematic due to low analyte surface coverage over the entire dynamic range. This was partially due to the fact that for all the above sensing strategies, a large label concentration was used to ensure the efficient labeling of the analyte.

In the theoretical calculations in cases 2–4, the sizes of the target analyte and label were assumed to be identical. However, in the case in which a nanoparticle label was significantly larger than the biomolecules (either the target analyte or the labeling biomolecule) within the dynamic range, the interaction of the surface-bound species was expected to be smaller than the interaction between the nanoparticle seeds. This would be due to the larger gap between biomolecules. Under these conditions, the Langmuir isotherm remained as a good model for describing the adsorption processes of analyte in the dynamic range. Theoretical results suggested that the dynamic range remained similar for different sizes of labeling seeds, as shown in Figure 9 for case 2

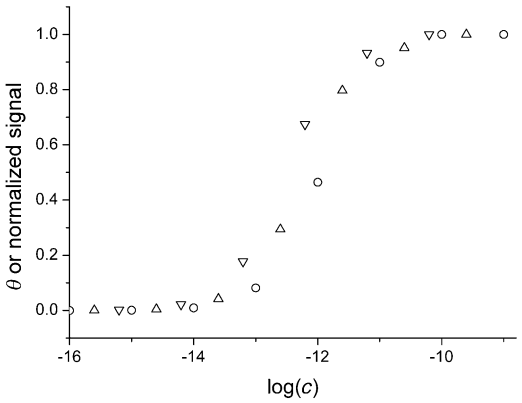

Figure 9. Effect of nanoparticle diameter: ○) 10 nm, △) 20 nm, and ▽) 40 nm, on the calibration curves of the biosensor. Nanoparticles are used as ultramicroelectrode array for the electrolysis of a large substrate concentration. $K = 1 \times 10^{8}$ м$^{-1}$, substrate diffusion coefficient $= 1 \times 10^{-5}$ cm^2 s^{-1}, and scan rate $= 0.1$ V s^{-1}.

whereby the diameters of the nanoparticle labels were 20 and 40 nm, and the diffusion coefficient of the substrate was 1×10^{-5} cm^2 s^{-1}. However, the location of the dynamic range appeared at a lower concentration than the cases considered above (shown in Figure 9). This was because the diffusion layer of large nanoparticle labels would start to overlap at a lower analyte surface coverage on account of the smaller gaps between these labels when there is an equal number of nanoparticle labels on the surface.

Alternatively, for the case in which the nanoparticle label is significantly smaller than the biomolecules (either the target analyte or the labeling biomolecule), the molecular interaction between the larger biomolecules could become important in the dynamic range whereby a reasonably large gap was present between the nanoparticle labels. In this case, the Frumkin isotherm would be a better approximation for the surface adsorption process of the analytes. The dynamic range of the biosensor was expected to vary depending on the type of interaction as discussed in case 1.

Detection limit and effect of nonspecific adsorption: In all cases, the detection limit was anticipated to be much lower after amplification under the ideal conditions whereby nonspecific adsorption was minimal. However, cases 2–4 have the potential for the signal to be overamplified. In these cases, the analyte surface coverage was very small throughout the dynamic range. Under these conditions, a small amount of nonspecific label adsorption could adversely impact the biosensor response, because a plateau would be reached with just a small number of nonspecifically adsorbed labels. As an example, nonspecific adsorption of as few as 40000 10 nm nanoparticles (surface coverage of 1×10^{-6}) in case 4 could trigger the deposition of a sufficient number of nanoparticles to produce a sensor response in the plateau range of the calibration curve.

Possible solutions: To overcome the above-mentioned obstacles faced in electrochemical biosensing that uses nanoparticles for signal amplification, the following solutions might be explored.

To develop sensing strategies that are sensitive enough to detect the physiochemical changes due to the binding of target analyte without excessive reliance on labels. Label-free detection strategies would not only simplify the sensing process, but also minimize the negative effect associated with the use of labels. However, the sensitivity of label-free electrochemical affinity biosensors is generally lower than biosensors that employ nanoparticle labels.

To discover biomolecules that can bind specifically and strongly to the analyte. In this instance, nonspecific adsorption of the labels would be minimized since a very low concentration of labels would be sufficient to ensure the complete labeling of the adsorbed target analytes. Moreover, a higher binding affinity would also allow for more stringent washing protocols so as to minimize nonspecific adsorption. In addition, a mild signal amplification strategy such as that mentioned in case 1 would be sufficient to achieve a high sensitivity according to the results presented in Figure 3. For the same considerations, implementation of a nonfouling surface (i.e., apart from the binding sites, ideally the rest of this surface is inert to any adsorption) for both the biosensing platform and nanoparticle labels would further minimize nonspecific adsorption of the labels.

A flow system can improve the biosensing process. In this case, the effect due to the transition from radial diffusion to linear diffusion could be minimized if the mass transport were mainly governed by convection for all analyte surface coverage conditions within the linear region of the calibration curve. In real sample testing processes, a small volume of developer solution would normally be used. In this situa-

tion, diffusion and depletion effects are expected to increase significantly on the timescale of the seed-mediated deposition process in cases 3 and 4 when the analyte surface coverage and the nanoparticle labels increase. As a consequence, the sensitivity and/or the slope of the dynamic range would decrease. This problem would be minimized if a flow system was used. Furthermore, the use of a flow system would also be helpful in decreasing the standard deviation introduced by the operator.

In the case of seed-mediated deposition, the process might switch from mass-transport-controlled to kinetics-controlled when a weaker reductant is used in the developer solution. Under such conditions, the effect of mass transport can be omitted. However, the sensitivity of the biosensor is expected to be lower in this case.

Finally, careful blank/background tests are always useful to ensure that the contribution from any nonspecific adsorption is minimal.

Conclusion

In this paper, theoretical studies have been conducted to investigate the analytical performance of amplified electrochemical affinity biosensors that use nanoparticle labels. Numerical simulations were used extensively to rigorously deal with the theoretical challenges. Although a high sensitivity could be achieved by using nanoparticle labels under all the conditions considered, the simulation results suggested that nonspecific adsorption would be considerable in amplified detection methods in which mass transport played an important role. This was because a mismatch existed between the surface chemistry of analyte binding and the principle of signal amplification. Under these conditions, the signal would plateau at a much lower concentration, well before the analyte binding reached a plateau. Possible solutions to these limitations have also been proposed.

Acknowledgements

This work was funded by the Institute of Bioengineering and Nanotechnology (Biomedical Research Council, Agency for Science, Technology and Research, Singapore). JZ would like to thank the Australian Research Council for support. The authors thank Dr. Yanbing Zu and Dr. Zhiqiang Gao for helpful discussions.

[1] E. Katz, I. Willner, *Electroanalysis* **2003**, *15*, 913–947.
[2] P. B. Luppa, L. J. Sokoll, D. W. Chan, *Clin. Chim. Acta* **2001**, *314*, 1–26.
[3] O. A. Sadik, O. Austin, A. O. Aluocha, A. Zhou, *Biosens. Bioelectron.* **2009**, *24*, 2749–2765.
[4] J. Wang, *Biosens. Bioelectron.* **2006**, *21*, 1887–1892.
[5] R. Gill, M. Zayats, I. Willner, *Angew. Chem.* **2008**, *120*, 7714–7736; *Angew. Chem. Int. Ed.* **2008**, *47*, 7602–7625.
[6] E. Katz, I. Willner, *Angew. Chem.* **2004**, *116*, 6166–6235; *Angew. Chem. Int. Ed.* **2004**, *43*, 6042–6108.
[7] E. Katz, I. Willner, J. Wang, *Electroanalysis* **2004**, *16*, 19–44.
[8] G. D. Liu, Y. H. Lin, *Talanta* **2007**, *74*, 308–317.
[9] S. Guo, S. Dong, *TrAC Trends Anal. Chem.* **2009**, *28*, 96–109.
[10] G. Liu, J. Wang, Y. Lin, J. Wang in *Electrochemical Sensors, Biosensors and Their Biomedical Applications, Chapter 14: Nanoparticle-Based Biosensors and Bioassays, Academic Press, Amsterdam*, **2008**, pp. 441–457.
[11] H. Fan, Z. Chang, R. Xing, M. Chen, Q. Wang, P. He, Y. Fang, *Electroanalysis* **2008**, *20*, 2113–2117.
[12] C. Ding, Q. Zhang, S. Zhang, *Biosens. Bioelectron.* **2009**, *24*, 2434–2440.
[13] A. Ambrosi, M. T. Castaneda, A. J. Killard, M. R. Smyth, S. Alegret, A. Merkoci, *Anal. Chem.* **2007**, *79*, 5232–5240.
[14] J. Wang, G. Liu, A. Merkoci, *J. Am. Chem. Soc.* **2003**, *125*, 3214–3215.
[15] H. Gao, J. Zhong, P. Qin, C. Lin, W. Sun, K. Jiao, *Microchim. Acta* **2009**, *165*, 173–178.
[16] J. A. Hansen, R. Mukhopadhyay, J. Ø. Hansen, K. V. Gothelf, *J. Am. Chem. Soc.* **2006**, *128*, 3860–3861.
[17] L. Authier, C. Grossiord, P. Brossier, *Anal. Chem.* **2001**, *73*, 4450–4456.
[18] N. Zhu, A. Zhang, Q. Wang, P. He, Y. Fang, *Electroanalysis* **2004**, *16*, 577–582.
[19] J. Wang, D. Xu, A. N. Kawde, R. Polsky, *Anal. Chem.* **2001**, *73*, 5576–5581.
[20] A. Numnuam, K. Y. Chumbimuni-Torres, Y. Xiang, R. Bash, P. Thavarungkul, P. Kanatharana, E. Pretsch, J. Wang, E. Bakker, *J. Am. Chem. Soc.* **2008**, *130*, 410–411.
[21] J. Zhang, B. P. Ting, N. R. Jana, Z. Gao, J. Y. Ying, *Small* **2009**, *5*, 1414–1417.
[22] B. P. Ting, J. Zhang, Z. Gao, J. Y. Ying, *Biosens. Bioelectron.*, **2009**, *25*, 282–287.
[23] J. Das, M. A. Aziz, H. Yang, *J. Am. Chem. Soc.* **2006**, *128*, 16022–16023.
[24] R. Polsky, R. Gill, L. Kaganovsky, I. Willner, *Anal. Chem.* **2006**, *78*, 2268–2271.
[25] R. Polsky, J. C. Harper, D. R. Wheeler, S. M. Dirk, J. A. Rawlings, S. M. Brozik, *Chem. Commun.* **2007**, 2741–2743.
[26] Z. Gao, Z. Yang, *Anal. Chem.* **2006**, *78*, 1470–1477.
[27] J. Zhang, J. Wang, J. Zhu, J. Xu, H. Chen, D. Xu, *Microchim. Acta* **2008**, *163*, 63–70.
[28] X. Chua, X. Fu, K. Chen, G. L. Shen, R. Q. Yu, *Biosens. Bioelectron.* **2005**, *20*, 1805–1812.
[29] S. Gupta, S. Huda, P. K. Kilpatrick, O. D. Velev, *Anal. Chem.* **2007**, *79*, 3810–3820.
[30] A. de la Escosura-Muñiz, M. M. D. Costa, A. Arben Merkoci, *Biosens. Bioelectron.* **2009**, *24*, 2475–2482.
[31] H. Cai, Y. Wang, P. He, Y. Fang, *Anal. Chim. Acta* **2002**, *469*, 165–172.
[32] T. M. H. Lee, L. L. Li, I. M. Hsing, *Langmuir* **2003**, *19*, 4338–4343.
[33] K. T. Liao, H. J. Huang, *Anal. Chim. Acta* **2005**, *538*, 159–164.
[34] M. Yang, C. Wang, *Anal. Biochem.* **2009**, *385*, 128–131.
[35] J. Wang, D. Xu, R. Polsky, *J. Am. Chem. Soc.* **2002**, *124*, 4208–4209.
[36] H. Cai, C. Shang, I. M. Hsing, *Anal. Chim. Acta* **2004**, *523*, 61–68.
[37] J. Wang, R. Polsky, D. Xu, *Langmuir* **2001**, *17*, 5739–5741.
[38] M. Rochelet-Dequaire, B. Limoges, P. Brossier, *Analyst* **2006**, *131*, 923–929.
[39] B. P. Ting, J. Zhang, M. Khan, Y. Y. Yang, J. Y. Ying, *Chem. Commun.* **2009**, 6231–6233.
[40] Y. Huang, W. Qian, J. H. Jiang, G. L. Shen, R. Q. Yu, *Biosens. Bioelectron.* **2008**, *24*, 600–605.
[41] B. Limoges, D. Marchal, F. Mavré, J. M. Savéant, B. Schöllhorn, *J. Am. Chem. Soc.* **2008**, *130*, 7259–7275.
[42] B. Limoges, D. Marchal, F. Mavré, J. M. Savéant, *J. Am. Chem. Soc.* **2008**, *130*, 7276–7285.
[43] A. J. Bard, L. R. Faulkner, *Electrochemical Methods: Fundamentals and Applications*, 2nd ed., John Wiley & Sons, New York, **2001**.
[44] M. Paunovic, M. Schlesinger, *Fundamental of Electrochemical Deposition*, , 2nd ed., Wiley, New York, **1998**..
[45] J. D. Norton, H. S. White, S. W. Feldberg, *J. Phys. Chem.* **1990**, *94*, 6772–6780.

[46] C. P. Smith, H. S. White, *Anal. Chem.* **1993**, *65*, 3343–3353.
[47] K. B. Oldham, J. C. Myland, *Fundamentals of Electrochemical Science*, Academic Press, San Diego, **1994**.
[48] P. R. Unwin, A. J. Bard, *J. Phys. Chem.* **1991**, *95*, 7814–7824.
[49] K. B. Oldham, *J. Electroanal. Chem. Interfacial Electrochem.* **1981**, *122*, 1–17.
[50] S. W. Feldberg, *J. Electroanal. Chem. Interfacial Electrochem.* **1981**, *127*, 1–10.
[51] D. J. Gavaghan, *J. Electroanal. Chem.* **1998**, *456*, 1–12.
[52] B. A. Brookes, D. J. Gavaghan, R. G. Compton, *J. Phys. Chem. B* **2002**, *106*, 4886–4896.
[53] A. Konash, A. R. Harris, J. Zhang, D. Elton, M. Hyland, G. Kennedy, A. M. Bond, *J. Solid State Electrochem.* **2009**, *13*, 551–563.
[54] X. Dai, G. G. Wildgoose, C. Salter, A. Crossley, R. G. Compton, *Anal. Chem.* **2006**, *78*, 6102–6108.
[55] T. J. Davies, R. R. Moore, C. E. Banks, R. G. Compton, *J. Electroanal. Chem.* **2004**, *574*, 123–152.
[56] T. J. Davies, B. A. Brookes, A. C. Fisher, K. Yunus, S. J. Wilkins, P. R. Greene, J. D. Wadhawan, R. G. Compton, *J. Phys. Chem. B* **2003**, *107*, 6431–6444.
[57] B. A. Brookes, T. J. Davies, A. C. Fisher, R. G. Evans, S. J. Wilkins, K. Yunus, J. D. Wadhawan, R. G. Compton, *J. Phys. Chem. B* **2003**, *107*, 1616–1627.
[58] C. Amatore, J. M. Savéant, D. Tessier, *J. Electroanal. Chem.* **1983**, *147*, 39–51.
[59] T. J. Davies, C. E. Banks, R. G. Compton, *J. Solid State Electrochem.* **2005**, *9*, 797–808.
[60] E. Budevski, G. Staikov, W. J. Lorenz, *Electrochim. Acta* **2000**, *45*, 2559–2574.
[61] N. R. Jana, L. Gearheart, C. J. Murphy, *Adv. Mater.* **2001**, *13*, 1389–1393.
[62] N. R. Jana, L. Gearheart, C. J. Murphy, *Langmuir* **2001**, *17*, 6782–6786.
[63] N. R. Jana, L. Gearheart, C. J. Murphy, *Chem. Mater.* **2001**, *13*, 2313–2322.
[64] B. Nikoobakht, M. A. El-Sayed, *Chem. Mater.* **2003**, *15*, 1957–1962.
[65] C. J. Murphy, T. K. San, A. M. Gole, C. J. Orendorff, J. X. Gao, L. Gou, S. E. Hunyadi, T. Li, *J. Phys. Chem. B* **2005**, *109*, 13857–13870.

Received: April 23, 2012
Revised: July 23, 2012
Published online: ■■ ▮▮, 0000

Biosensors

J. Zhang, B. P. Ting,*
*J. Y. Ying** ..... ▮▮▮▮–▮▮▮▮

Theoretical Assessment of Binding and Mass-Transport Effects in Electrochemical Affinity Biosensors That Utilize Nanoparticle Labels for Signal Amplification

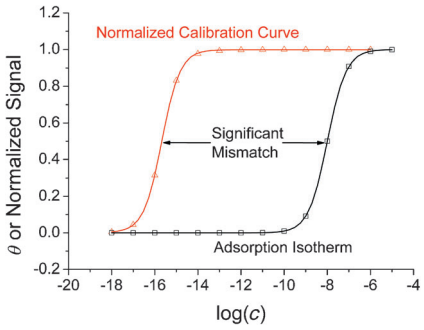

Mis-matchmaker: A significant mismatch between the calibration curve and adsorption isotherm can occur when mass transport plays an important role in electrochemical signal amplification (see figure). This can lead to a dramatic interference of nonspecific adsorption of labels in the measurements.

